

# NATURE OF STOCHASTIC ION HEATING IN THE SOLAR WIND: TESTING THE DEPENDENCE ON PLASMA BETA AND TURBULENCE AMPLITUDE

DANIEL VECH<sup>1</sup>, KRISTOPHER G. KLEIN<sup>1,2</sup> AND JUSTIN C. KASPER<sup>1</sup>,

<sup>1</sup>Climate and Space Sciences and Engineering, University of Michigan, Ann Arbor, MI 48109, USA, <sup>2</sup>Lunar and Planetary Laboratory, University of Arizona, Tucson, AZ 85719, USA; dvech@umich.edu

## ABSTRACT

The solar wind undergoes significant heating as it propagates away from the Sun; the exact mechanisms responsible for this heating are not yet fully understood. We present for the first time a statistical test for one of the proposed mechanisms, stochastic ion heating. We use the amplitude of magnetic field fluctuations near the proton gyroscale as a proxy for the ratio of gyroscale velocity fluctuations to perpendicular (with respect to the magnetic field) proton thermal speed, defined as  $\epsilon_p$ . Enhanced proton temperatures are observed when  $\epsilon_p$  is larger than a critical value ( $\sim 0.019 - 0.025$ ). This enhancement strongly depends on the proton plasma beta ( $\beta_{\parallel p}$ ); when  $\beta_{\parallel p} \ll 1$  only the perpendicular proton temperature  $T_{\perp}$  increases, while for  $\beta_{\parallel p} \sim 1$  increased parallel and perpendicular proton temperatures are both observed. For  $\epsilon_p$  smaller than the critical value and  $\beta_{\parallel p} \ll 1$  no enhancement of  $T_p$  is observed while for  $\beta_{\parallel p} \sim 1$  minor increases in  $T_{\parallel}$  are measured. The observed change of proton temperatures across a critical threshold for velocity fluctuations is in agreement with the stochastic ion heating model of Chandran et al. (2010). We find that  $\epsilon_p > \epsilon_{\text{crit}}$  in 76% of the studied periods implying that stochastic heating may operate most of the time in the solar wind at 1 AU.

*Keywords:* plasmas — turbulence — solar wind — waves

## 1. INTRODUCTION

The solar wind is a hot, tenuous plasma propagating away from Sun's surface. The radial expansion of the solar wind is highly non-adiabatic with the proton temperature cooling significantly slower than a spherically expanding ideal gas (e.g. Wolfe et al. 1966; Hundhausen et al. 1970). The radial dependence of proton temperature  $T_p$  as a function of the heliocentric distance  $r$  is measured on the average as  $r^{-0.74}$  compared to  $r^{-4/3}$  corresponding to adiabatic expansion (Hellinger et al. 2011). This slow decay of the temperature is consistent with the solar wind undergoing significant heating. Identifying the physical mechanisms responsible for this heating and quantifying their contribution as a function of plasma and solar wind parameters is fundamentally important to describing the solar corona and solar wind and to characterizing heating in plasma systems more generally. Several mechanisms have been proposed to heat the solar wind as it expands, including cyclotron damping (Cranmer 2000), magnetic reconnection (Drake et al. 2009; Osman et al. 2012, 2014; Greco et al. 2016; Mistry et al. 2017), Landau damping (Leamon et al. 1999; Cranmer et al. 2007; Gary & Nishimura 2004) and stochastic heating (McChesney et al. 1987; Johnson & Cheng 2001; Chaston et al. 2004; Voitenko

& Goossens 2004; van der Holst et al. 2014).

This Letter focuses on stochastic ion heating: such heating occurs when the motion of ions becomes chaotic as the amplitude of electromagnetic field fluctuations at scales comparable to the ion gyroscale exceed a critical value. Under these conditions, the magnetic moment of ions is not conserved, allowing diffusion in energy perpendicular to the magnetic field and leading to perpendicular heating of the ions. Stochastic heating may have a significant contribution to the ion heating in coronal holes and the solar wind, however its importance relative to other mechanisms is an open question. Coronagraph measurements have shown that minor ions such as O<sup>+5</sup> originating from coronal holes have significantly larger perpendicular temperature  $T_{\perp}$  (with respect to the magnetic field) than parallel  $T_{\parallel}$  (Kohl et al. 1998; Antonucci et al. 2000). In situ observations of the fast solar wind frequently find similar proton temperature anisotropy of  $T_{\perp}/T_{\parallel} > 1$  (e.g. Marsch et al. 2004; Hellinger et al. 2006).

Chandran et al. (2010) modeled ion stochastic heating by low frequency ( $\omega < \Omega_p$ , where  $\omega$  and  $\Omega_p$  denote the wave and proton cyclotron frequencies, respectively) Alfvén (AW) and kinetic Alfvén waves (KAW). They proposed that the heating rate of this mechanism is very sensitive to the amplitude of the turbulent velocity fluc-

tuations, which they characterized by the dimensionless parameter  $\epsilon_i = \delta v_\rho / v_\perp$  where  $\delta v_\rho$  denotes the amplitude of root-mean-square velocity fluctuations at scales comparable to the ion gyroscale while  $v_\perp$  is the ion's thermal speed perpendicular to the background magnetic field. When the velocity fluctuations are smaller than some critical value,  $\epsilon_i \ll \epsilon_{\text{crit}}$ , the magnetic moment of the ions is conserved and any stochastic heating is suppressed. When  $\epsilon_i \gtrsim \epsilon_{\text{crit}}$  magnetic moment conservation is violated, leading to energy diffusion perpendicular to the magnetic field and an increase in  $T_\perp$ . In test particle simulations from Chandran et al. (2010)  $\epsilon_{\text{crit}}$  was reported as 0.19. Chandran et al. (2010) predicted that depending on the values of  $\beta_{\parallel p}$  (ratio of parallel thermal pressure to magnetic pressure;  $n_p k_B T_{\parallel p} / (B_0^2 / 2\mu_0)$ , where  $n_p$  denotes the proton density,  $k_B$  is the Boltzmann constant,  $T_{\parallel p}$  is the parallel proton temperature,  $B_0$  is the magnitude of the magnetic field, and  $\mu_0$  is the permeability of free space) the following proton heating behaviors are expected under the assumption of low-frequency, KAW-like turbulence:

1. If  $\beta_{\parallel p} \ll 1$  and  $\epsilon_p \ll \epsilon_{\text{crit}}$ , electrons absorb the vast majority of the cascade power and proton heating is negligible as the Landau resonance condition ( $\omega - k_{\parallel} v_{\parallel} = 0$ , where  $k_{\parallel}$  and  $v_{\parallel}$  denote the parallel wavenumber and particle velocity along the magnetic field direction, respectively) is not satisfied for protons. (Quataert 1998; Gruzinov 1998).
2. If  $\beta_{\parallel p} \ll 1$  and  $\epsilon_p \gtrsim \epsilon_{\text{crit}}$ , stochastic ion heating operates and AW/KAW turbulence causes both electron and perpendicular proton heating while the parallel proton heating is negligible.
3. If  $\beta_{\parallel p} \sim 1$  and  $\epsilon_p \ll \epsilon_{\text{crit}}$ , electron and parallel proton heating occurs due to Landau damping and transit-time damping of KAWs. Stochastic heating is suppressed producing no increase in the perpendicular proton temperature.
4. If  $\beta_{\parallel p} \sim 1$  and  $\epsilon_p \gtrsim \epsilon_{\text{crit}}$ , stochastic heating operates and the electrons and protons both receive significant fractions of the cascade power, with similar energy transferred to both perpendicular and parallel proton temperatures.

Bourouaine & Chandran (2013) tested the predictions of Chandran et al. (2010) studying 3 days of Helios-2 measurements with radial distances ranging from 0.29-0.64 AU, focusing on fast solar wind with low plasma beta ( $\beta < 0.3$ ). Stochastic heating by low-frequency AW/KAW turbulence was consistent with the observed perpendicular temperature in the solar wind for the three selected intervals. Xia et al. (2013) performed fur-

ther tests of the model of Chandran et al. (2010), describing test particles interacting with strong reduced magnetohydrodynamic (RMHD) turbulence. RMHD was found to be much more effective at stochastic heating than randomly phased waves used in previous studies. They suggested that stochastic heating can occur not only under  $\beta \ll 1$  conditions of the solar corona but also when  $\beta \sim 1$ , typically occurring at 1 AU. Klein & Chandran (2016) modeled the evolution of proton distributions due to stochastic heating in the range of 4 to 30 solar radii, finding that the proton distributions developed non-Gaussian structures characterized with a flat core and steep tail.

Despite these works, the role of stochastic heating in the solar wind is not yet fully understood. In particular no statistical study using solar wind observations has been carried out to test the effect of low-frequency AW/KAWs on proton heating. In this Letter, we present the analysis of 13 years of Wind data to investigate scalar proton and electron temperatures and proton temperature anisotropy as a function of  $\beta$  and turbulence amplitude. We expect and find positive correlation between the turbulence amplitude and  $T_p$ , in agreement with previous studies (e.g. Grappin et al. 1990; Cranmer & Van Ballegoijen 2005; Wu et al. 2013; Matthaeus et al. 2016; Hughes et al. 2017a,b), suggesting that the damping mechanism requires a higher amplitude of the fluctuations in order to operate. We explicitly compare the observed features to the expected behavior of stochastic heating and find the proton temperature depends on a critical turbulence amplitude in agreement with the predictions of Chandran et al. (2010).

## 2. METHOD

### 2.1. Background

The goal of the data analysis was to organize temperature measurements as a function of  $(\epsilon_p, \beta_{\parallel p})$  and compare the temperature dependence of these parameters with the predictions of stochastic ion heating. Following the methodology of Bourouaine & Chandran (2013), we define the velocity fluctuations at the proton gyroscale,  $\delta v_p$ , as

$$\delta v_p = \sigma v_A \delta B_p / B_0 \quad (1)$$

where  $\sigma = 1.19$  is a dimensionless constant arising from the KAW dispersion relation,  $v_A = B_0 / \sqrt{\mu_0 \rho}$  denotes the Alfvén speed,  $\rho$  is the mass density of the solar wind, and  $\delta B_p$  is the amplitude of magnetic field fluctuations at proton gyroscale. This approximation is necessary as observations of velocity fluctuations have not yet been made at sufficiently high cadences to resolve  $\delta v_p$  except in unusual solar wind conditions. In Equation 1,  $\delta B_p$  is

obtained by evaluating

$$\delta B_p = \frac{\pi}{C_\gamma} \left[ \int_{e^{-0.5}f_\rho}^{e^{0.5}f_\rho} P_f(f) df \right]^{1/2} \quad (2)$$

where  $P_f(f)$  denotes the observed turbulent spectrum of magnetic fluctuations,  $f_\rho$  is the frequency corresponding to the proton gyroradius defined as  $V_{SW} \sin(\Theta_{VB})/2\pi\rho_p$ , where  $V_{SW}$  is the speed of the solar wind,  $\Theta_{VB}$  is the angle between the solar wind velocity vector and the magnetic field and  $\rho_p$  is the proton gyroradius. The dimensionless parameter  $C_\gamma$  arises from the integral  $\int_0^{\pi/2} (\cos\phi)^{\gamma-1} d\phi$ , and is defined as

$$C_\gamma = \frac{\sqrt{\pi}\Gamma\left[\frac{\gamma}{2}\right]}{2\Gamma\left[\frac{\gamma+1}{2}\right]} \quad (3)$$

where  $\gamma$  is the absolute value of the spectral index of the turbulent spectrum within the integration limits. An extensive discussion of using magnetic fluctuation frequency spectra as a proxy for gyroscale velocity fluctuations can be found in Appendices A and B of [Bourouaine & Chandran \(2013\)](#).

Equation 2 assumes that  $C_\gamma$  is constant within the integration limits, meaning that the spectral index  $\gamma$  does not change in the given frequency range. This requirement is violated when the break frequency  $f_b$  is within the integration limits,  $e^{-0.5}f_\rho < f_b < e^{0.5}f_\rho$ . [Bourouaine & Chandran \(2013\)](#) restricted their analysis to 3 intervals when the integration limits were above the break of the turbulent spectrum,  $f_b < e^{-0.5}f_\rho$ . As we aim to use a statistical approach, we employ the following approximation when  $f_b$  is within the integration limits of Equation 2. We replace  $C_\gamma$  in Equation 2 with  $\bar{C}_\gamma$ , the weighted average of  $C_\gamma$  below and above  $f_b$ :

$$\bar{C}_\gamma = \frac{C_{\gamma 1} \int_{e^{-0.5}f_\rho}^{f_b} P_f(f) df + C_{\gamma 2} \int_{f_b}^{e^{0.5}f_\rho} P_f(f) df}{\int_{e^{-0.5}f_\rho}^{f_b} P_f(f) df + \int_{f_b}^{e^{0.5}f_\rho} P_f(f) df} \quad (4)$$

where  $C_{\gamma 1,2}$  is calculated separately for the spectral indices above and below  $f_b$  using Equation 3. This approximation is used in 31% percent of the intervals. Given  $\delta B_p$  calculated from Equations 2 and 4, we calculate  $\epsilon_p = \delta v_p/v_\perp$  using Equation 1 and the perpendicular proton thermal speed  $v_\perp = \sqrt{2k_B T_\perp/m_p}$ .

## 2.2. Application

In this study, high resolution Wind magnetic field data (92 ms cadence) ([Lepping et al. 1995](#)) were used together with onboard ion moments and ion parameters (92 second cadence) from the Faraday cup instrument ([Lin et al. 1995](#); [Ogilvie et al. 1995](#)). Data from January 2004 to December 2016 were selected to ensure Wind was in the pristine solar wind. For the analysis, the

magnetic field and plasma data were split in 10-minute intervals. The power spectral density (PSD) of the magnetic field components were calculated separately using Fourier transform and then the component PSDs were added to obtain the total PSD ([Koval & Szabo 2013](#)). The time series of  $\beta_{\parallel p}$ ,  $T_{\parallel}$ ,  $T_\perp$  and electron temperature ( $T_e$ ) were averaged over the 10-minute periods. Overall,  $\sim 5.8 \cdot 10^5$  turbulent spectrums and corresponding average solar wind parameters were computed. Due to gaps in the data, only  $\sim 5.2 \cdot 10^5$  average electron temperatures were obtained.

For the correct calculation of  $C_\gamma$  and  $\bar{C}_\gamma$  (Equations 3-4), it was necessary to estimate  $f_b$ , which shows some variability ranging from 0.1-1 Hz ([Markovskii et al. 2008](#); [Chen et al. 2014](#); [Franci et al. 2016](#); [Telloni & Bruno 2016](#)) making its parameterization difficult. To automatically estimate this frequency, we developed the following algorithm: starting from 0.1 Hz until 5.17 Hz a grid of 43 logarithmically spaced frequencies was generated. For each PSD, 33 linear fits were made in the frequency range between the  $i^{th}$  and  $i+10^{th}$  element of the grid. From the ensemble of fits, the steepest spectral index and the corresponding frequency range were selected. The average and standard deviation of the measured spectra indices are  $-2.99 \pm 0.65$ , in very good agreement with previous studies on the dissipation range from [Leamon et al. \(1998\)](#) and [Smith et al. \(2006\)](#).

The frequency range corresponding to the steepest part of the spectrum can be used very effectively to estimate  $f_b$ , which is shown in Figure 1a and b. A typical magnetic field turbulent spectrum is presented in Figure 1a. The steepest part of the spectrum (corresponding to the dissipation range) was detected automatically with our algorithm and is marked with a black line. The red circles denote the 33 spectral indices in the range of 0.1 – 5.17 Hz. In Figure 1b, we investigate how well this method could be used as a proxy for  $f_b$  on a statistical basis. A histogram of the low frequency end of the dissipation range is illustrated, based on all the available  $\sim 5.8 \cdot 10^5$  data points. The distribution has a peak at around 0.3 Hz, decaying rapidly toward larger frequencies with only 0.8% of the distribution having  $f_b$  larger than 1 Hz (not shown). There is a secondary peak between 0.1-0.126 Hz, the majority of these spectrums did not display a well-defined high frequency break because the spectrum flattened immediately after the inertial range due to reaching the noise floor ([Koval & Szabo 2013](#)). This occurs when the amplitude of the inertial scale magnetic field fluctuations are very small, reducing the power level of the spectrum. The measurements in the range of 0.1-0.126 Hz ( $\sim 11\%$  of the overall spectrums) shown in Figure 1b were excluded from the study. The remaining frequencies had a median value of 0.3 Hz, which is in very good agreement with the study

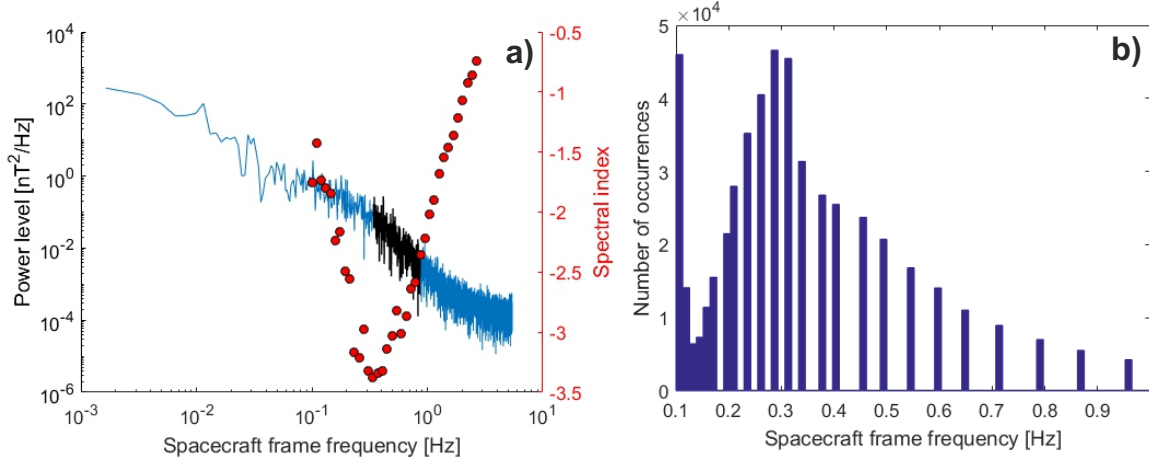


**Figure 1.** (a) an example of the measured magnetic turbulent spectrums and the measured spectral indices (red marks) in the 0.1-5.17 Hz range; (b) histogram of the low frequency end of the measured dissipation ranges (black part of the spectrum in panel a) for all the  $\sim 5.8 \cdot 10^5$  periods.

**Table 1.** Comparison of  $\delta B_p$ ,  $\delta v_p$  and  $\epsilon_p$  from Bourouaine & Chandran (2013) with the values presented in our study

Parameter	Measurements at 0.29, 0.4 and 0.64 AU	Median value of our study at 1 AU
$\delta B_p$ [nT]	1.16; 0.70; 0.32	0.20
$\delta v_p$ [km/s]	5.15; 4.13; 3.21	2.34
$\epsilon_p$	0.0471; 0.0486; 0.0480	0.0520

of Markovskii et al. (2008) who manually inspected 454 magnetic turbulent spectrums and found that the median of  $f_b$  was approximately 0.3 Hz. They also found that  $f_b$  was larger than 1 Hz in 2.1% of the cases and it was lower than 0.1 Hz in 4.3% of the cases.

To accurately evaluate the integral in Equation 2, the unphysical flattening of the high frequency part of the spectrum must be considered. In the cases when the high frequency end of the integration limit  $e^{0.5} f_\rho$  was outside the dissipation range (black region in Figure 1a) linear extrapolation was used to estimate the power of the turbulent spectrum at  $f_\rho$  (Bourouaine & Chandran 2013). When  $f_b$  was within the integration limits of Equation 2, linear fits were used in the ranges of  $[e^{-0.5} f_\rho, f_b]$  and  $[f_b, e^{0.5} f_\rho]$  to calculate  $\gamma_{1,2}$  and  $\bar{C}_\gamma$ . The integration of Equation 2 was done with trapezoid technique to obtain  $\delta B_p$ . Table 1 compares the results of Bourouaine & Chandran (2013) in the range of 0.29 – 0.64 AU with the median values calculated from our study.

### 3. RESULTS

In order to study the proton temperature distribution, a grid with 50 x 25 equally logarithmic spaced bins was generated in the  $(\epsilon_p, \beta_{||p})$  space. The scalar proton temperature  $((T_{||} + 2T_{\perp})/3)$ , proton temperature anisotropy

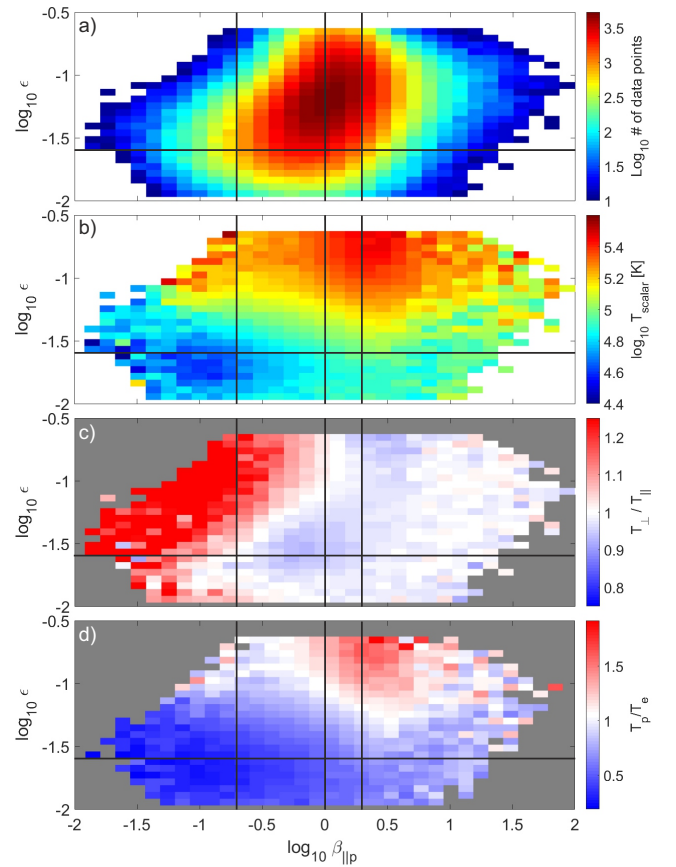


**Figure 2.** Data distribution (a), median values of the scalar proton temperature (b), proton temperature anisotropy (c) and proton-electron temperature ratio (d) in the  $(\epsilon_p, \beta_{||p})$  space. Horizontal line at  $\epsilon_p = 10^{-1.6}$  denotes the point where stochastic heating starts operating. Vertical lines at  $\beta = 0.2, 1$  and  $2$  mark the cross sections, which are highlighted in Figure 3.

$(T_{\perp}/T_{||})$  and ratio of the scalar proton and electron temperature  $(T_p/T_e)$  were binned in the defined grid. The median value of each bin was selected and sparse bins

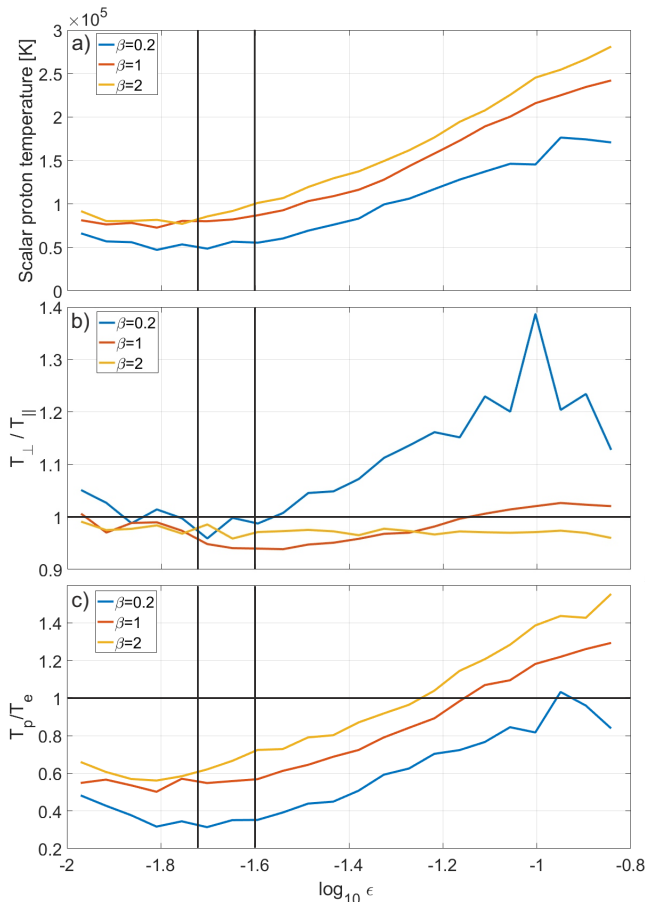


**Figure 3.** Cross sections of Figure 2a, b and c along  $\beta_{\parallel p} = 0.2, 1$  and  $2$ , respectively.

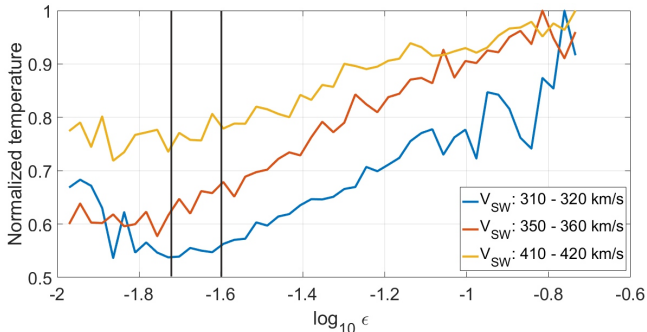


**Figure 4.** Cross sections of the binned  $T_p$  data in the  $(\epsilon_p, V_{SW})$  space along three solar wind speed intervals. Each  $T_p$  line was normalized to its peak value.

with less than 10 data points were excluded from the study. To avoid the possible effect of outliers, we excluded the lowest and highest 1% of  $\epsilon_p$  values.

Figure 2a shows the distribution of the data peaking at  $\beta_{\parallel p} = 0.99$  and  $\epsilon = 0.0520$ . The color bars in Figure 2b, c and d show the binned scalar proton temperature (on logarithmic scale), proton temperature anisotropy (on linear scale) and proton-electron temperature ratio (on linear scale), respectively. Cross sections of Fig-

ure 2b, c and d along  $\beta_{\parallel p} = 0.2, 1$  and  $2$  (marked with vertical lines) as a function of  $\epsilon_p$  are shown in Figure 3a, b and c, respectively. The scalar proton temperature in Figure 2b shows a clear dependence on  $\epsilon_p$  and a sharp increase in the temperature can be seen at approximately  $\epsilon_p = 10^{-1.6}$ , marked with a black line. When  $\epsilon_p$  is smaller than  $10^{-1.6}$  the temperature is around  $5 \cdot 10^4$  K while for  $\epsilon_p > 10^{-1.6}$  the peak temperature is  $3.1 \cdot 10^5$  K.  $\epsilon_p > 10^{-1.6}$  occurred in 76% of the  $\sim 5.8 \cdot 10^5$  studied intervals. The  $\beta_{\parallel p}$  dependence of the scalar proton temperature is shown in Figure 3a: in all cases a sudden temperature enhancement can be seen when  $\epsilon_p$  is in the range of  $10^{-1.72}$  and  $10^{-1.6}$  (marked with vertical lines).

In Figure 2c, the proton temperature anisotropy increases as a function of  $\epsilon_p$  when  $\beta_{\parallel p} < 1$  while no significant systematic trend can be seen for  $\beta_{\parallel p} > 1$ . In Figure 3b the cross section at  $\beta_{\parallel p} > 0.2$  shows some variations around  $T_{\perp}/T_{\parallel} = 1$  when  $\epsilon_p < 10^{-1.6}$ . For  $\epsilon_p > 10^{-1.6}$  there is a significant increase in the perpendicular proton temperature, resulting in  $T_{\perp}/T_{\parallel} \sim 1.20$ . In the case of  $\beta_{\parallel p} = 1$  and  $\epsilon_p < 10^{-1.6}$ ,  $T_{\perp}/T_{\parallel}$  shows minor preference for an enhanced parallel temperature ( $T_{\perp}/T_{\parallel} \sim 0.96$ ) while for  $\epsilon_p > 10^{-1.6}$   $T_{\perp}/T_{\parallel}$  approaches unity.

The  $T_p/T_e$  distribution in Figure 2d shows similarities to the scalar proton temperature in Figure 2b, with the ratio strongly depending on  $\epsilon_p$ , having its lowest values for  $\epsilon_p < 10^{-1.6}$ . Similar to Figure 3a and b, the cross sections in panel c show a sudden increase of the  $T_p/T_e$  ratio at  $\epsilon_p = 10^{-1.6}$ . When  $\beta_{\parallel p} = 0.2$  the proton and electron temperatures are in equilibrium ( $T_p/T_e = 1$ ) for the largest  $\epsilon_p$  values while for  $\beta_{\parallel p} = 1$ , protons have a factor of 1.2 higher temperature than electrons.

$T_p$  is known to be a strong function of the solar wind speed (e.g. Burlaga & Ogilvie 1973; Richardson & Smith 2003), which may affect the observed temperature variations in the  $(\epsilon_p, \beta_{\parallel p})$  space. To investigate this speed dependence the  $T_p$  data was binned in the  $(\epsilon_p, V_{SW})$  space and cross sections were taken along three solar wind speed intervals. The results are shown in Figure 4 where each line was normalized to its peak  $T_p$  value. The temperature variations as a function of  $\epsilon_p$  are consistent with Figures 2-3 and show a sudden enhancement at approximately  $\epsilon_p = 10^{-1.6}$  indicating that  $T_p$  does have a dependence on  $\epsilon_p$  in addition to the dependence on  $V_{SW}$ .

We note that  $\epsilon_p \propto 1/\sqrt{T_{\perp}}$  and  $\beta_{\parallel p} \propto T_{\parallel}$ . If only this intrinsic dependence of the variables was significant we would expect the highest  $T_p$  at the lowest  $\epsilon_p$ , and for a fixed  $\beta_{\parallel p}$ ,  $T_{\perp}/T_{\parallel}$  would decrease as a function of  $\epsilon_p$ . Neither of these tendencies are observed in Figures 2 or 3, implying that the amplitude of the turbulent fluctuations is the primary driver of the magnitude of  $\epsilon_p$ .

## 4. CONCLUSION

In this Letter, we have provided the first statistical test for the presence of stochastic ion heating of the type predicted by Chandran et al. (2010). Our findings are consistent with the prediction that stochastic heating becomes effective once gyroscale velocity fluctuations surpass a critical amplitude leading to perpendicular proton heating. We found that the critical  $\epsilon_p$  value in our study is in the range of 0.019 and 0.025 and that 76% of the studied intervals had an  $\epsilon_p$  value larger than 0.025, consistent with stochastic ion heating operating nearly continuously in the solar wind at 1 AU. Based on the distribution of the temperature data in the  $(\epsilon_p, \beta_{||p})$  space, we make the following conclusions:

1. If  $\beta_{||p} = 0.2$  and  $\epsilon_p \ll \epsilon_{\text{crit}}$  the lowest scalar proton temperatures ( $\sim 5 \cdot 10^4$  K) were measured. The majority of the turbulent energy is absorbed by electrons as shown by the low  $T_p/T_e$  ratios observed for this case.
2. If  $\beta_{||p} = 0.2$  and  $\epsilon_p \gtrsim \epsilon_{\text{crit}}$ , an increase in the perpendicular proton temperature was identified, with  $T_{\perp}/T_{||} \sim 1.20$  for the largest values of  $\epsilon_p$ . The scalar proton temperature increased by a factor of 3 compared to the  $\beta_{||p} = 0.2, \epsilon_p \ll \epsilon_{\text{crit}}$  case.
3. If  $\beta_{||p} = 1$  and  $\epsilon_p \ll \epsilon_{\text{crit}}$ , no preferential perpendicular heating was observed ( $T_{\perp}/T_{||} \sim 0.96$ ), consistent with non-stochastic heating from AW/KAW turbulence.
4. If  $\beta_{||p} = 1$  and  $\epsilon_p \gtrsim \epsilon_{\text{crit}}$ , no preferential increase in  $T_{\perp}$  was identified ( $T_{\perp}/T_{||} \sim 1.01$ ) and the scalar proton temperature reached  $1.58 \cdot 10^5$  K, a factor

of 3 increase compared to the  $\beta_{||p} = 1, \epsilon_p \ll \epsilon_{\text{crit}}$  case.

The findings above qualitatively agree with the predictions of Chandran et al. (2010), which is the main result of this Letter. We do note that our observed value of  $\epsilon_{\text{crit}}$  is an order of magnitude smaller than that reported by Chandran et al. (2010), which arises from a prediction for when more than half of the cascade power near  $k_{\perp}\rho_p = 1$  is absorbed by stochastic heating; see their Equations 25, 30, and 31. Their calculation depends sensitively on several dimensionless parameters characterizing the turbulent fluctuations. Variation in these parameters may be sufficient to explain the discrepancy in the value of  $\epsilon_{\text{crit}}$ .

Another potential explanation for this discrepancy arises from Kasper et al. (2017) suggesting that a majority of preferential minor ion heating occurs within a zone some tens of solar radii from the Sun's surface. It is plausible that the same mechanism preferentially heating the minor ions also heats the protons and a significant fraction of the energy transfer occurs within the preferential heating zone. Thus, the  $\epsilon_{\text{crit}}$  observed at 1 AU may not be the actual threshold for the onset of stochastic heating, but rather a value to which  $\epsilon_{\text{crit}}$  has decayed. Similarly, the observed correlation between  $\epsilon_p$  and  $T$  may be a remnant of heating closer to the Sun, with plasma which underwent stochastic heating and retained relatively high values of temperature and  $\epsilon_p$  compared to other plasma measured at 1 AU.

K.G. Klein was supported by NASA grant NNX16AM23G. J.C. Kasper was supported by NASA Grant NNX14AR78G. Data were sourced from CDAWeb (<http://cdaweb.gsfc.nasa.gov/>).

## REFERENCES

- Antonucci, E., Dodero, M. A., & Giordano, S. 2000, *Solar Physics*, 197, 115
- Bourouaine, S., & Chandran, B. D. 2013, *The Astrophysical Journal*, 774, 96
- Burlaga, L., & Ogilvie, K. 1973, *Journal of geophysical research*, 78, 2028
- Chandran, B. D., Dennis, T. J., Quataert, E., & Bale, S. D. 2011, *The Astrophysical Journal*, 743, 197
- Chandran, B. D., Li, B., Rogers, B. N., Quataert, E., & Germaschewski, K. 2010, *The Astrophysical Journal*, 720, 503
- Chandran, B.D.G., Verscharen, D., Quataert, E., Kasper, J.C., Isenberg, P.A., & Bourouaine, S. 2013, *The Astrophysical Journal*, 776, 45
- Chaston, C., Bonnell, J., Carlson, C., et al. 2004, *Journal of Geophysical Research: Space Physics*, 109
- Chen, C., Leung, L., Boldyrev, S., Maruca, B., & Bale, S. 2014, *Geophysical research letters*, 41, 8081
- Cranmer, S. R. 2000, *The Astrophysical Journal*, 532, 1197
- Cranmer, S. R. & Van Ballegooijen, A. A., 2005, *The Astrophysical Journal Supplement Series*, 156, 265
- Cranmer, S. R., Van Ballegooijen, A. A., & Edgar, R. J. 2007, *The Astrophysical Journal Supplement Series*, 171, 520
- Drake, J., Swisdak, M., Phan, T., et al. 2009, *Journal of Geophysical Research: Space Physics*, 114
- Franci, L., Landi, S., Matteini, L., Verdini, A., & Hellinger, P. 2016, *The Astrophysical Journal*, 833, 91
- Gary, S. P., & Nishimura, K. 2004, *Journal of Geophysical Research: Space Physics*, 109
- Grappin, R., Mangeney, A. & Marsch, E. 1990, *Journal of Geophysical Research: Space Physics*, 95, 8197-8209
- Greco, A., Perri, S., Servidio, S., Yordanova, E. & Veltri, P. 2016, *APJ*, 823, 2
- Gruzinov, A. V. 1998, *The Astrophysical Journal*, 501, 787
- Hellinger, P., Matteini, L., Štverák, Š., Trávníček, P. M., & Marsch, E. 2011, *Journal of Geophysical Research: Space Physics*, 116
- Hellinger, P., Trávníček, P., Kasper, J. C., & Lazarus, A. J. 2006, *Geophysical research letters*, 33
- Hughes, R.S., Gary, S.P., & Wang, J. 2017, *ApJL*, 835, 1

- Hughes, R.S., Gary, S.P., Wang, J., & Parashar, T.N. 2017, *ApJL*, 847, 2
- Hundhausen, A., Bame, S., Asbridge, J., & Sydoriak, S. 1970, *Journal of Geophysical Research*, 75, 4643
- Johnson, J. R., & Cheng, C. 2001, *Geophysical research letters*, 28, 4421
- Kasper, J., Klein, K., Weber, T., et al. 2017, *the Astrophysical Journal*
- Klein, K. G., & Chandran, B. D. 2016, *The Astrophysical Journal*, 820, 47
- Kohl, J., Noci, G., Antonucci, E., et al. 1998, *The Astrophysical Journal Letters*, 501, L127
- Koval, A., & Szabo, A. 2013in , *AIP*, 211–214
- Leamon, R. J., Smith, C. W., Ness, N. F., Matthaeus, W. H., & Wong, H. K. 1998, *Journal of Geophysical Research: Space Physics*, 103, 4775
- Leamon, R. J., Smith, C. W., Ness, N. F., & Wong, H. K. 1999, *Journal of Geophysical Research: Space Physics*, 104, 22331
- Lepping, R., Acuña, M., Burlaga, L., et al. 1995, *Space Science Reviews*, 71, 207
- Lin, R., Anderson, K., Ashford, S., et al. 1995, *Space Science Reviews*, 71, 125
- Markovskii, S., Vasquez, B. J., & Smith, C. W. 2008, *The Astrophysical Journal*, 675, 1576
- Marsch, E., Ao, X.-Z., & Tu, C.-Y. 2004, *Journal of Geophysical Research: Space Physics*, 109
- Matthaeus, W., Parashar, T.N., Wan, M. & Wu, P. 2016, *ApJL*, 827, 1
- McChesney, J., Stern, R., & Bellan, P. 1987, *Physical Review Letters*, 59, 1436
- Mistry, R., J. P. Eastwood, T. D. Phan, and H. Hietala 2017, *JGR*, 122, 58955909
- Ogilvie, K., Chornay, D., Fritzenreiter, R., et al. 1995, *Space Science Reviews*, 71, 55
- Osman, K.T., Matthaeus, W.H., Hnat, B., Chapman, Sandra, C., 2012, *Physical Review Letters*, 108, 261103
- Osman, K.T., Matthaeus, W.H., Gosling, J.T., Greco, A., et al. 2014, *Physical Review Letters*, 112, 215002
- Quataert, E. 1998, *The Astrophysical Journal*, 500, 978
- Richardson, J. D., & Smith, C. W. 2003, *Geophysical research letters*, 30
- Smith, C. W., Hamilton, K., Vasquez, B. J., & Leamon, R. J. 2006, *The Astrophysical Journal Letters*, 645, L85
- Telloni, D., & Bruno, R. 2016, *Monthly Notices of the Royal Astronomical Society: Letters*, 463, L79
- van der Holst, B., Sokolov, I. V., Meng, X., et al. 2014, *The Astrophysical Journal*, 782, 81
- Voitenko, Y., & Goossens, M. 2004, *The Astrophysical Journal Letters*, 605, L149
- Wolfe, J. H., Silva, R. W., & Myers, M. A. 1966, *Journal of Geophysical Research*, 71, 1319
- Wu, P, Wan, M, Matthaeus, WH, Shay, MA & Swisdak, M. 2013, *Physical review letters*, 111, 121105
- Xia, Q., Perez, J. C., Chandran, B. D., & Quataert, E. 2013, *The Astrophysical Journal*, 776, 90